

Impurity invisibility in graphene: Symmetry guidelines for the design of efficient sensors

John Duffy and James Lawlor
School of Physics, Trinity College Dublin, Dublin 2, Ireland

Caio Lewenkopf
Instituto de Física, Universidade Federal Fluminense, 24210-346 Niterói RJ, Brazil

Mauro S. Ferreira
*School of Physics, Trinity College Dublin, Dublin 2, Ireland and
CRANN, Trinity College Dublin, Dublin 2, Ireland*
(Dated: July 12, 2021)

Renowned for its sensitivity to detect the presence of numerous substances, graphene is an excellent chemical sensor. Unfortunately, which general features a dopant must have in order to enter the list of substances detectable by graphene are not exactly known. Here we demonstrate with a simple model calculation implemented in three different ways that one of such features is the symmetry properties of the impurity binding to graphene. In particular, we show that electronic scattering is suppressed when dopants are bound symmetrically to both graphene sub-lattices, giving rise to impurity invisibility. In contrast, dopants that affect the two sublattices asymmetrically are more strongly scattered and therefore the most likely candidates to being chemically sensed by graphene. Furthermore, we demonstrate that impurity invisibility is lifted with the introduction of a symmetry-breaking perturbation such as uniaxial strain. In this case, graphene with sublattice-symmetric dopants will function as efficient strain sensors. We argue that by classifying dopants through their bonding symmetry leads to a more efficient way of identifying suitable components for graphene-based sensors.

PACS numbers: 72.80.Vp, 73.23.-b, 72.10.-d, 73.63.-b

I. INTRODUCTION

Due to its well-documented physical properties and numerous applications, graphene has been in the scientific limelight for over a decade now¹⁻⁴. Due to its linear dispersion relation graphene shows some quite unique transport phenomena, such as Klein tunnelling, manifest as a suppression of backscattering⁵⁻⁷. Here we focus on one of the more exciting features of graphene is the extreme sensitivity of its transport properties to relatively low disorder or impurity concentrations⁸⁻¹³. This makes graphene an attractive material for use in sensor-based applications, and indeed there has already been a lot of research in this direction, confirming its ability to detect substances at ultra-low concentrations (sub-PPM)¹⁴⁻²¹.

Which substances can graphene detect is a question that continues driving the search for atoms and molecules that impact its transport properties. This search has been mainly based on trial and error, *i.e.*, by exposing graphene to a variety of dopants in the hope that they function as strong scattering centres^{11,22-26}. Owing to the overwhelming number of possibilities to account for, it is no surprise that this *ad-hoc* approach fails to provide insight on the conditions that ideal dopants must have to make good graphene-based sensors. Rather than trial and error, a more general approach is needed to guide the search for efficient sensors.

With that goal in mind, this study makes use of a simple model calculation that describes the electronic scat-

tering in impurity-doped graphene. Rather than specifying the exact form and detailed characteristics of the doping impurities, we adopt a more general approach that aims to separate the distinct contributions to scattering events: one that depends on the intrinsic specificity of dopants and another that is determined primarily by their bonding symmetry. Whereas there is an enormous variety of impurities that interact with graphene, there are only a few different conformations that characterize the bonding symmetry. Remarkably, out of this small number of symmetries, we show that there is one in particular that gives rise to vanishingly small scattering regardless of the specific details of the dopant. This class of dopants is therefore expected to be hardly visible for the conduction electrons.

This finding corresponds to a considerable advance from the aforementioned *ad-hoc* strategy since we are able to infer about the graphene properties of a whole range of dopants that have this particular bonding symmetry. Most importantly, because the predicted weak-scattering behaviour is symmetry-dependent, any symmetry-breaking perturbation is likely to enhance the scattering strength of this class of impurities. Therefore, we argue that graphene doped with impurities that have this particular bonding symmetry will give rise to devices that are extremely sensitive to, for instance, uniaxial mechanical strain.

Regarding the sequence adopted in this manuscript, we start by defining the model Hamiltonian, followed by

a few different yet complementary ways of accounting for the scattering contribution of impurities in graphene. All these approaches lead to the same conclusion, *i.e.*, that impurities with certain bonding symmetries may be completely transparent, causing hardly any electronic scattering. We finish by discussing possible consequences that this feature might bring to the field of sensor design.

II. MODEL HAMILTONIAN

Let us define the model Hamiltonian used throughout the manuscript. The system consists of a graphene sheet with one single impurity described by the Hamiltonian $H = H_0 + V$, where

$$H_0 = - \sum_{\langle i,j \rangle} |i\rangle t_{i,j} \langle j| + \sum_{\langle \ell,m \rangle} |\ell\rangle h_{\ell,m} \langle m| \quad (1)$$

corresponds to the pristine nearest-neighbour tight-binding graphene Hamiltonian defined by the matrix elements $t_{i,j}$ plus a single impurity defined by the matrix elements $h_{\ell,m}$. The indices i and j label the graphene sites while ℓ and m label the impurity sites. The states $|\alpha\rangle$ represent an atomic orbital centred at site α , where $\alpha = \{i, j, \ell, m\}$. The matrix elements $t_{i,j} = t$ when i and j are nearest neighbours and vanish otherwise. The value of $t = 2.7$ eV is known to reproduce well the low energy electronic structure of graphene and will hereafter serve as our energy unit. Although not specified, the matrix elements $h_{\ell,m}$ may describe a variety of possible impurities ranging from single atoms to more complex structures such as molecules and nanoparticles. The only assumptions made about the impurity is that it connects to graphene through only one of its sites (labelled $\ell = 0$) and that the orbital $|0\rangle$ possesses certain symmetries. These assumptions can be easily relaxed, should we need to consider impurities of a more complex geometrical structure and/or with orbitals of different symmetries^{27,28}.

Note that H_0 describes a graphene sheet and a single impurity totally decoupled from one another. The graphene-impurity coupling term is described by V and depends on the bonding conformation. We assume that impurities can be either centre-, top- or bridge-bonded to the graphene lattice, as schematically depicted in Fig. 1. For the sake of completeness, we also include substitutional impurities in the figure because their scattering response is practically identical to top-bonded impurities.

The coupling operator V , now renamed V_T , V_B and V_C depending on the conformation type, is defined as

$$V_T = |0\rangle \tau \langle 1| + \text{H.c.} \quad (2)$$

$$V_B = |0\rangle \tau_1 \langle 1| + |0\rangle \tau_2 \langle 2| + \text{H.c.} \quad (3)$$

$$V_C = \sum_{i \in \text{R}} |0\rangle \tau_i \langle i| + \text{H.c.} , \quad (4)$$

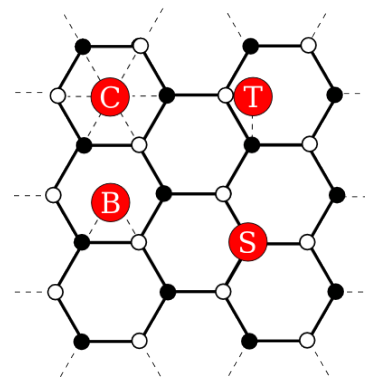


FIG. 1. (Color online) Schematic representation of a centre-bonded (labelled with a C); a top-bonded (labelled with a T); and a bridge-bonded (labelled with a B) impurity. For the sake of completeness, we also include a schematic representation of a substitutional impurity (labelled with an S). Impurities are represented by red circles while filled and hollow circles correspond to the two graphene sublattices also referred to as A and B sublattices.

where the subscripts T , B and C refer to top, bridge and centre, respectively. The state $|0\rangle$ represents an orbital centred at the impurity site that is bonded to the graphene sheet, whereas the others are orbitals centred on graphene sites. In the center bonded case, the sum runs over the six carbon sites of the hexagonal ring R surrounding the impurity.

In the case of centre-bonded impurities, the values of τ_i depend on how the impurity hybridizes with the graphene atoms. The possibilities are^{27,28}: (i) It may hybridize equally with all six neighboring carbon atoms ($\tau_i = \tau$), which is the case for s and d_{z^2} orbitals; (ii) It may have a π -phase difference in the hybridization of the adsorbed impurity with the two different sublattices, ($\tau_1 = \tau_3 = \tau_5 = -\tau_2 = -\tau_4 = -\tau_6 \equiv \tau$), which is typical of f orbitals; (iii) For a d_{xy} orbital, $\tau_1 = \tau_4 = 0$ and $\tau_2 = \tau_5 = -\tau_3 = -\tau_6 = \sqrt{3}\tau/2$; (iv) For a $d_{x^2-y^2}$ orbital, $\tau_1 = \tau_4 = \tau$ and $\tau_2 = \tau_3 = \tau_5 = \tau_6 = -\tau/2$. Here we focus on the first two possibilities, where the values of $|\tau_i|$ are the same for all i .

III. IMPURITY SCATTERING

Having defined the model Hamiltonian, three distinct approaches will be used to study how the graphene conductance is impacted by the introduction of different bonding-symmetry impurities. First we investigate how the scattering events are described by the real-space Green functions of impurity-doped graphene. We then turn our attention to writing the scattering cross section in wave-number domain and analyze how it is affected by the introduction of graphene dopants. Finally, the conductance of doped graphene is numerically calculated through the Kubo formula. These complementary meth-

ods shed light on different aspects of the scattering process and how the electronic transport is affected by the bonding-symmetry of the dopants.

A. Scattering in real space

It is convenient to describe the scattering processes associated to adsorbed impurities in graphene in terms of the T -matrix. The latter is defined by $G = g + gTg$, where $G = (E - H)^{-1}$ the system full Green's function and $g = (E - H_0)^{-1}$ is the free Green's function. The T -matrix can be obtained from the Dyson equation, $G = g + gVG$, using standard Green's function techniques²⁹.

This strategy allows us calculate the electronic propagator between two arbitrary graphene sites a and b in the presence of the graphene-impurity coupling term. The simplest case to consider is of top-bonded impurities described by V_T . Here,

$$G_{a,b} = g_{a,b} + g_{a,1} T_T g_{1,b}, \quad (5)$$

where

$$T_T = \Sigma(1 - g_{11}\Sigma)^{-1} \quad (6)$$

is the relevant T -matrix element and

$$\Sigma \equiv |\tau|^2 g_{0,0}, \quad (7)$$

where $g_{0,0}$ is the uncoupled impurity Green's function projected on $|0\rangle$. Σ acts as the self-energy associated with the impurity.

Scattering is fully described by the second term on the r.h.s. of Eq. (5). It is worth noting that the part of the T -matrix that depends on the specific details of the impurity is entirely contained in the self-energy, *i.e.*, in the “contact” Green function $g_{0,0}$. Therefore, scattering caused by any top-bonded impurity is fully taken into account by Eq. (5) once the Green function $g_{0,0}$ is known.

Similar steps are followed to obtain the propagator $G_{a,b}$ for bridge- and centre-bonded impurities, taking care to replace V_T by V_B and V_C , respectively. The corresponding full Green's functions are given by

$$G_{a,b} = g_{a,b} + (g_{a,1} + g_{a,2}) T_B (g_{1,b} + g_{2,b}), \quad (8)$$

and

$$G_{a,b} = g_{a,b} + (g_{a,1} + \dots + g_{a,6}) T_C (g_{1,b} + \dots + g_{6,b}), \quad (9)$$

respectively. The T -matrix for the bridge- and the centre-bonded impurities are denoted, respectively, by T_B and T_C . They read

$$T_B = \Sigma(1 - \gamma_B \Sigma)^{-1} \quad (10)$$

and

$$T_C = \Sigma(1 - \gamma_C \Sigma)^{-1}, \quad (11)$$

where $\gamma_B = \sum_{i,j=1}^2 g_{ij}$ and $\gamma_C = \sum_{i,j=1}^6 g_{ij}$ are sums of all the matrix elements of g involving graphene sites that are bonded to the impurity. γ_B involves a sum over 4 terms and γ_C a sum over 36 terms.

A simple analysis of Eq. (5) indicates that, for top-bonded impurities, the scattering contribution to the propagator $\Delta G_{a,b} \equiv G_{a,b} - g_{a,b}$ contains the usual product of three quantities: (i) one off-diagonal propagator $g_{a,1}$ between site a and the scattering site on graphene, (ii) the relevant matrix element of the T -matrix and (iii) another off-diagonal propagator $g_{1,b}$ this time associated with site b . In this case, the only way the scattering can be weak is if the T_T itself is small, *i.e.*, if the top-bonded impurity is a weak scatterer.

The situation changes for bridge- and centre-bonded impurities, described respectively by Eqs. (8) and (9). The scattering correction of the propagator is still written as a product of three separate terms, one of which being the T -matrix. The other two terms involve not one single propagator but a sum of several propagators g . More specifically, the sums $\alpha_B = g_{a,1} + g_{a,2}$ and $\beta_B = g_{1,b} + g_{2,b}$ appear in Eq. (8) while the sums $\alpha_C = g_{a,1} + \dots + g_{a,6}$ and $\beta_C = g_{1,b} + \dots + g_{6,b}$ can be seen in Eq. (9).

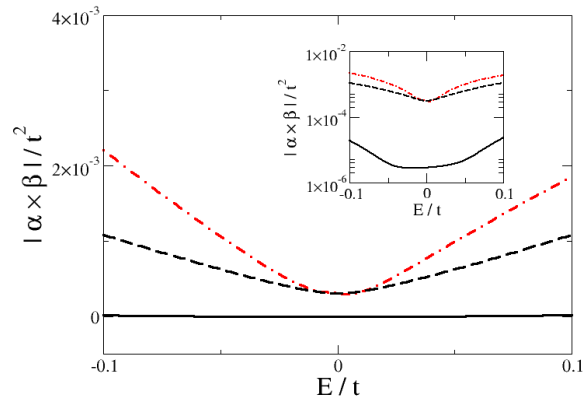


FIG. 2. (Color online) Scattering contribution to the single-particle Green function $|\alpha \times \beta|$ (in units of t^{-2}) as a function of the energy (in units of the electron hopping t). The (black) solid line corresponds to the case of centre-bonded impurities described by Eq. (9); the (black) dashed line is for bridge-bonded impurities described by Eq. (8) and the (red) dot-dashed line represents the case of top-bonded impurities according. Note that in the case of top-bonded impurities the product $\alpha \times \beta = g_{a,1} \times g_{1,b}$. The inset shows the same results in a linear-log plot.

The sums in α_C and β_C give rise to interference effects that strongly modify ΔG_{ab} . To investigate the magnitude of the interference contribution, we show in Fig. 2 results for the product $|\alpha_B \times \beta_B|$ and $|\alpha_C \times \beta_C|$, for bridge- and centre-bonded impurities, respectively. These results are for impurities halfway between sites a and b , chosen to be a distance $20 a_0$ apart along the armchair direction,

where a_0 is the graphene lattice parameter. Sites a and b are arbitrarily chosen carbon atoms on the graphene lattice and the results shown in Fig. 2 are not qualitatively affected by any specific choice of their values. For the sake of comparison, we also plot the equivalent product $|g_{a,1} \times g_{1,b}|$ seen in Eq. (5) for the case of top-bonded impurities. Results are plotted as a function of the electron energy. While all curves have a minimum at the Dirac point, the most revealing aspect of this figure is what happens to the curves as the energy moves away from $E = 0$. Results for top- and bridge-bonded impurities increase fairly rapidly, but the centre-bonded case is remarkably different. The quantity $\alpha_C \times \beta_C$ is orders of magnitude smaller than the other two cases and clearly indicates that the sums $(g_{a,1} + \dots + g_{a,6})$ and $(g_{1,b} + \dots + g_{6,b})$ vanish as a result of destructive interference in the propagators g . The log-scale plot in the inset of Fig. 2 shows that the centre-bonded results are between 2 and 3 orders of magnitude weaker than the other two cases. The same could have been concluded by using the analytical expression for the off-diagonal matrix elements of the graphene Green's function within the tight-binding approximation³⁰.

A direct consequence of the results shown in Fig. 2 is that centre-bonded impurities, except for the d -orbital ones, are very weak scatterers. The generality of our argument is based on the fact that even without specifying what impurities are being considered, the destructive interference experienced by the propagators in Eq. (9) will give rise to results that are orders of magnitude smaller than those obtained by Eqs. (5) and Eq. (8). Note that this effect occurs regardless of the value of the real-space T -matrix T_C , unless of course the T -matrix has resonance levels at very specific energies. We address the issue of resonances in Sec. III C.

B. Scattering cross section

We now turn our attention to the cross section of graphene in the presence of top-bonded (σ_T) and centre-bonded (σ_C) impurities. Results for bridge-bonded impurities will not be pursued simply because, as seen in Fig. 2, they behave very similarly to the case of top-bonded dopants.

The cross section is directly related to the T -matrix. In scattering theory, the T -matrix is usually defined

$$V|\psi_E^{(+)}\rangle = T^+(E)|\mathbf{k}\rangle, \quad (12)$$

where $|\psi_E^{(+)}\rangle$ is a solution of the Lippmann-Schwinger equation, namely

$$|\psi_E^{(+)}\rangle = |\mathbf{k}\rangle + g^+(E)V|\psi_E^{(+)}\rangle. \quad (13)$$

We are interested in the scattering amplitude $f_{\text{scat}}(\mathbf{k}, \mathbf{k}') \sim \langle \mathbf{k}|T|\mathbf{k}'\rangle$, that is directly related to the scattering cross-section and the transport time that

appears in the Boltzmann equation used in the analysis of the transport properties of graphene in the diffusive regime^{3,5,6}. The fundamental difference to the previous section is that here we express all key quantities in the wave-number basis, as opposed to the real-space basis.

Recalling that the tight-binding Hamiltonian for pristine graphene can be written in momentum representation as

$$H_{0,\text{graphene}} = t \begin{pmatrix} 0 & f(\mathbf{k}) \\ f^*(\mathbf{k}) & 0 \end{pmatrix}, \quad (14)$$

where

$$f(\mathbf{k}) = -(e^{-i\mathbf{k}\cdot\mathbf{a}_1} + e^{-i\mathbf{k}\cdot\mathbf{a}_2} + 1). \quad (15)$$

The corresponding eigenstates read³¹

$$|\mathbf{k}, \pm\rangle = \frac{1}{\sqrt{2}} \sum_n e^{i\mathbf{k}\cdot\mathbf{R}_n} \left(|n, A\rangle \pm e^{i\theta(\mathbf{k})} |n, B\rangle \right), \quad (16)$$

where $+$ ($-$) corresponds to positive (negative) eigenenergies, $\mathbf{R}_n = \mathbf{R}_n^A$, and $\theta(\mathbf{k}) = \arg[f(\mathbf{k})]$. A and B refer to the two equivalent graphene sublattices. Note that $|\mathbf{k}, \pm\rangle$ are scattering states normalized to a Dirac delta-function, and, consequently, that have a different normalization than the states defined in Ref. 31.

Since $|\mathbf{k}\rangle$ distinguishes between A and B sites, we introduce the lattice labelling defined in Fig. 3. The primitive unit cell consists of a pair of A and B sites connected by a vertical bond. The PUCs are defined as $i = (m, n)$ with $\mathbf{R}_i = m\mathbf{a}_1 + n\mathbf{a}_2$.

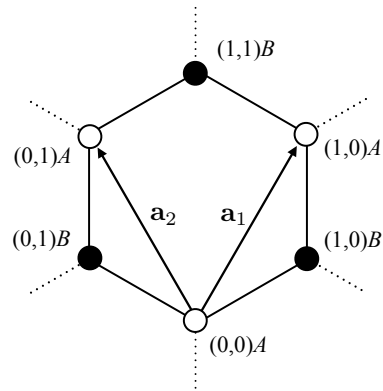


FIG. 3. Schematic representation of the lattice labels $i = (m, n)$ corresponding to $\mathbf{R}_i = m\mathbf{a}_1 + n\mathbf{a}_2$. For the top-bonded case, the impurity is placed atop of the $(0,0)$ site, whereas for the center-bonded case, the impurity is at the center of the hexagonal ring.

For top-bonded impurities, the explicit representation of the T -matrix operator in the site basis is

$$T_T = |i\rangle\langle i|T_T|i\rangle\langle i| = \mathcal{T}_T(E) \sum_i |i\rangle\langle i|. \quad (17)$$

For a single top-absorbed impurity, we write

$$\begin{aligned} \langle \mathbf{k}', \pm | T_T | \mathbf{k}, \pm \rangle &= \frac{1}{2} \sum_{i,j} e^{-i\mathbf{k}' \cdot \mathbf{R}_i + i\mathbf{k} \cdot \mathbf{R}_j} \\ &\times \left(\langle i, A | \pm e^{i\theta(\mathbf{k}')} \langle i, B | \right) T_T \left(| j, A \rangle \pm e^{-i\theta(\mathbf{k})} | j, B \rangle \right). \end{aligned} \quad (18)$$

Hence, if i belongs to the A sublattice we obtain

$$\langle \mathbf{k}', \pm | T_T | \mathbf{k}, \pm \rangle = \frac{\mathcal{T}_T(E)}{2} e^{-i(\mathbf{k}' - \mathbf{k}) \cdot \mathbf{R}_i} \quad (19)$$

while if i belongs to the B sublattice

$$\langle \mathbf{k}', \pm | T_T | \mathbf{k}, \pm \rangle = \frac{\mathcal{T}_T(E)}{2} e^{-i(\mathbf{k}' - \mathbf{k}) \cdot \mathbf{R}_i} e^{i\theta(\mathbf{k}') - i\theta(\mathbf{k})}. \quad (20)$$

The results for T_T are then further simplified by identifying the i site as $(0, 0)$ in the notation of Fig. 3. Note that if one is interested in coherent multiple scattering due to a finite concentration of impurities, the relative phases are important. Let us restrict ourselves to the low impurity concentration, where coherent multiple scattering is unlikely to play a significant role.

As a result,

$$\langle \mathbf{k}', \pm | T_T | \mathbf{k}, \pm \rangle = \frac{\mathcal{T}_T(E)}{2} \quad (21)$$

for $i \in A$ and

$$\langle \mathbf{k}', \pm | T_T | \mathbf{k}, \pm \rangle = \frac{\mathcal{T}_T(E)}{2} e^{i\theta(\mathbf{k}') - i\theta(\mathbf{k})} \quad (22)$$

The above expression yields 36 terms to compute. After a long, but straightforward calculation, one obtains

$$\langle \mathbf{k}', + | T_C | \mathbf{k}, + \rangle = \frac{\mathcal{T}_C(E)}{2} \left[f(\mathbf{k}') + e^{i\theta(\mathbf{k}')} e^{-i\mathbf{k} \cdot (\mathbf{a}_1 + \mathbf{a}_2)} f^*(\mathbf{k}') \right] \left[f^*(\mathbf{k}) + e^{-i\theta(\mathbf{k})} e^{i\mathbf{k}' \cdot (\mathbf{a}_1 + \mathbf{a}_2)} f(\mathbf{k}) \right], \quad (25)$$

for positive energies.

For low energies, it is convenient to expand the wave vectors around the K -points³, namely, $\mathbf{k} = \mathbf{K}^\xi + \mathbf{q}$ and $\mathbf{k}' = \mathbf{K}^\xi + \mathbf{q}'$, where $\xi = \pm$ is the valley index. For what follows it is useful to recall that

$$\mathbf{K}^\xi \cdot \mathbf{a}_1 = \frac{2\pi}{3}\xi \quad \text{and} \quad \mathbf{K}^\xi \cdot \mathbf{a}_2 = -\frac{2\pi}{3}\xi. \quad (26)$$

Note that $\mathbf{k} \cdot (\mathbf{a}_1 + \mathbf{a}_2) = \mathbf{K}^\xi \cdot (\mathbf{a}_1 + \mathbf{a}_2) + \mathbf{q} \cdot (\mathbf{a}_1 + \mathbf{a}_2) = 3aq_y$.

Expanding $f(\mathbf{k})$ to first order in \mathbf{q} , one obtains

$$f_\xi(\mathbf{k}) = \frac{3}{2} qa e^{-i\theta_\xi(\mathbf{q})} \quad (27)$$

where

$$e^{-i\theta(\mathbf{k})} \equiv e^{-i\theta_\xi(\mathbf{q})} = \xi \frac{q_x}{q} + i \frac{q_y}{q}. \quad (28)$$

We are now ready to conclude the calculation of the

for $i \in B$. The difference is just a phase, which is immaterial for the cross section. Despite not affecting the cross section for top-bonded dopants, this phase difference will have a dramatic effect when impurities are coupled equally to both A - and B -sublattices, as we demonstrate next.

Following similar steps, we now derive the wave-vector dependent T -matrix associated with centre-bonded impurities. For a single-impurity this quantity is expressed in the real-space basis by

$$T_C = \sum_{(i,j) \in R} |i\rangle \langle i| T_C |j\rangle \langle j| = \mathcal{T}_C(E) \sum_{(i,j) \in R} |i\rangle \langle j|. \quad (23)$$

Hence, for an impurity centred at the R th hexagon, one has

$$\begin{aligned} \langle \mathbf{k}', \pm | T_C | \mathbf{k}, \pm \rangle &= \frac{1}{2} \sum_{i,j \in R} e^{-i\mathbf{k}' \cdot \mathbf{R}_i + i\mathbf{k} \cdot \mathbf{R}_j} \\ &\times \left(\langle iA | \pm e^{i\theta(\mathbf{k}')} \langle iB | \right) T_C \left(| jA \rangle \pm e^{-i\theta(\mathbf{k})} | jB \rangle \right). \end{aligned} \quad (24)$$

k -dependent T -matrix, namely

$$\begin{aligned} \langle \mathbf{q}' \xi' + | T_C | \mathbf{q} \xi + \rangle &= \mathcal{T}_C(E) \frac{9a^2}{4} qq' e^{i[\theta_{\xi'}(\mathbf{q}') - \theta_\xi(\mathbf{q})]/2} \\ &\times \left\{ \cos 3[\theta_{\xi'}(\mathbf{q}') - \theta_\xi(\mathbf{q})] + \cos 3[\theta_{\xi'}(\mathbf{q}') + \theta_\xi(\mathbf{q})] \right\}, \end{aligned} \quad (29)$$

where $|\mathbf{k}+\rangle \equiv |\mathbf{q}\xi+\rangle$.

Two immediate conclusions can be extracted from Eq. (29): (i) The angular part of the scattering cross section displays the familiar $2\pi/3$ -periodicity that is inherent to the hexagonal symmetry of graphene; (ii) the T -matrix scales as $(qa)^2$ for low energies for both intra ($\xi = \xi'$) and intervalley ($\xi \neq \xi'$) scattering. The latter conclusion reiterates the results shown in Sec. III A and demonstrates once again that centre-bonded impurities hardly affect the transport properties of electrons near

the Dirac point.

It is worth emphasizing that this is a situation where a short-range impurity, taking into account intra- and intervalley scattering process, is suppressed by interference effects. This is quite different from the standard picture inferred from the scattering analysis of the Dirac equation in graphene, where one identifies the suppression of backscattering with long-range impurities and as a manifestation of Klein tunneling⁵.

C. Numerical results

We now study resonance scattering regime and the case of finite impurity-doped graphene systems, that involve multiple scattering. For that purpose we numerically calculate the conductance using the Kubo formula. The zero bias conductance Γ reads³²⁻³⁴

$$\Gamma = \frac{4e^2}{\hbar} \text{ReTr} \left[\tilde{\mathbf{G}}_{00} \mathbf{U}_{01} \tilde{\mathbf{G}}_{11} \mathbf{U}_{10} - \mathbf{U}_{01} \tilde{\mathbf{G}}_{10} \mathbf{U}_{10} \tilde{\mathbf{G}}_{10} \right] \quad (30)$$

where $\tilde{\mathbf{G}}_{j,\ell} = (\mathbf{G}_{j,\ell}^- - \mathbf{G}_{j,\ell}^+)/2i$ is the difference between the retarded and advanced Green functions. Here, $\mathbf{G}_{j,\ell}^\pm$ is the matrix formed by the Green function elements connecting unit cells j and ℓ . For computational purposes it is convenient to define a finite-sized graphene sample across which the conductance is calculated. In practice, this comes down to defining three graphene nanoribbons of similar width, two of which are semi-infinite and act as leads, separated by a finite-length section where impurities are placed. The indices 0 and 1 correspond to the interface between the central region and one of the leads. By taking the boundary conditions properly, this method gives the same results as the standard recursive Green's function method³⁵. Unit cells are defined as lines across the ribbon width and the trace is taken over both site and spin indices. Similarly, $\mathbf{U}_{j,\ell}$ represents a matrix consisting of off-diagonal hopping terms connecting neighboring unit cells j and ℓ . All Green functions above are evaluated at E_F .

Rather than treating the scatterers as general objects described by the self-energy definition of Eq. (7) as before, we must now specify the impurity in order to evaluate the conductance. We consider impurities with on-site energy ϵ_a , which modifies the self-energy Σ to

$$\Sigma = |\tau|^2 (E - \epsilon_a)^{-1}. \quad (31)$$

Figure 4 shows numerically evaluated results for the change in the conductance of a 8-atom wide graphene ribbon due to the presence of a single impurity as a function of the Fermi energy. Solid (dashed) line is for a centre-bonded (top-bonded) impurity. Top-bonded impurities are strong scatterers when compared to their centre-bonded counterparts. The dashed line shows that the conductance with top-bonded impurities is significantly reduced across a wide range of energies.

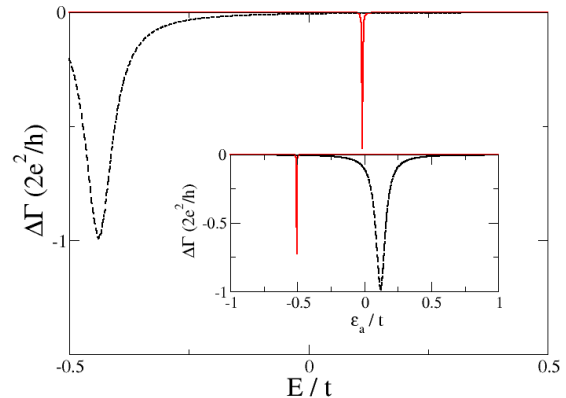


FIG. 4. (Color online) Change in the conductance $\Delta\Gamma$ (in units of $2e^2/h$) as a function of the Fermi energy for a single impurity with on-site energy $\epsilon_a = -0.5t$, and $\tau = -0.5t$. Solid red (dashed black) line corresponds to the case of a centre-bonded (top-bonded) impurity. Inset depicts the same quantity for a fixed Fermi energy $E_F = 0.11t$, this time plotted as a function of the impurity's on-site energy.

In contrast, the conductance of graphene with centre-bonded impurities is practically identical to that of the pristine case, except for a very narrow energy range around the resonance. This corroborates the preceding argument that the centre-bonded symmetry makes impurities with this type of bonding hardly visible to the conduction electrons. The narrow peak seen in the main panel of Fig. 4 is explained by Eq. (9). While the quantity $\alpha_C \times \beta_C$ approaches zero, as seen in Fig. 2, it is possible to find a suitable Fermi energy that leads to $\gamma_C \times \Sigma \approx 1$. When that happens the T -matrix T_C in Eq. (11) diverges, compensating the destructive interference effects. However, this is practically accidental and calls for some fine tuning of the Fermi energy and/or of the impurity resonance values, neither of which are very practical.

To make this point more explicitly, in the inset of Fig. 4 we have also show $\Delta\Gamma$ plotted as a function of the impurity on-site energy for a fixed E_F . Once again, an extremely narrow isolated peak suggests that the lack of transparency of centre-bonded impurities is not a robust feature but results from a coincidental match of energies.

In fact, in a recent paper, García and collaborators²⁸ studied the Anderson localization driven by adatom disorder in graphene. They find that despite the suppression of the scattering cross section due to destructive interference in center adsorbed impurities, the system undergoes an Anderson metal-insulator transition but only for particular values of the doping and the impurity resonance energy. Our results evidence that such a transition requires a very precise parameter tuning.

Instead of considering single impurities, we now pro-

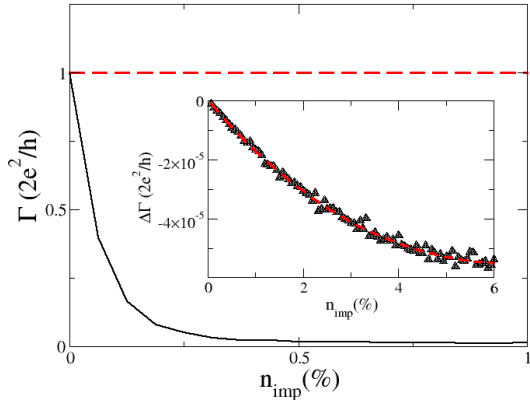


FIG. 5. Conductance (in units of $2e^2/h$) as a function of the impurity concentration n_{imp} . Solid (dashed) line corresponds to the case of top-bonded (centre-bonded) impurities. $E_F = 0$, $\tau = -2t$ and $\epsilon_a = 0.3t$. Inset shows the change in conductance $\Delta\Gamma$, indicating that the conductance actually decreases with increasing n_{imp} , but extremely slowly. All points were averaged over 1000 configurations.

ceed to studying how the conductance Γ changes as the impurity concentration n_{imp} increases, as shown in Fig. 5. Extensive configurational averaging was carried out to obtain statistical significance in our calculations. A very small percentage (0.01%) of top-bonded impurities (dashed line) is sufficient to reduce the conductance of a graphene ribbon to 50% of its pristine value whereas no reduction can be seen for centre-bonded scatterers (solid line). To perceive any reduction in the case of centre-bonded impurities, concentrations must exceed the 5% mark and yet the reduction is orders of magnitude smaller than that seen for the top-bonded symmetry case. The inset shows the change in conductance for centre-bonded impurities and reductions are practically negligible, confirming once again our ideas of impurity invisibility. When searching for experimental signatures of the distinct responses of top- and centre-bonded impurities, the results of Fig. 5 are the most evident.

IV. DISCUSSION AND CONCLUSIONS

Having demonstrated that the centre-bonded symmetry indeed gives rise to impurity transparency, it is worth now discussing what repercussions this finding brings. For a start, one may conclude that graphene can function as a good sensor of substances whose contact to the underlying hexagonal structure resembles that of top-bonded impurities. More specifically, it should be sensitive to the presence of impurities whose binding to the graphene sublattices is asymmetric, *i.e.*, the effect that the impurity causes to the graphene sublattices is different. As shown in Figs. 2, 4, and 5, the scattering caused

by top-bonded impurities is always the largest of all analyzed cases (for the same hybridization matrix element). This in itself is a valuable finding since it may offer a clear guideline in the search for substances that graphene can detect instead of the common *ad-hoc* approach of trial and error.

Another consequence is that centre-bonded impurities are not ideal for generating chemical sensors since they may be transparent. Nevertheless, they may be employed in the construction of sensors of a different nature. Because the impurity transparency results from a symmetry-driven destructive interference in the scattering cross section, all one needs to do to turn transparent objects into opaque scatterers is to break the perfect bipartite symmetry of the system. This can be easily achieved with uniaxial strain³⁶.

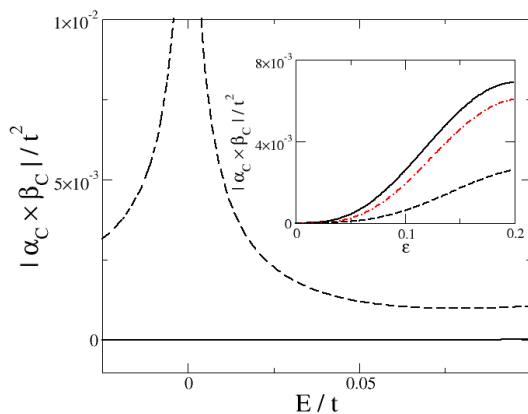


FIG. 6. $|\alpha_C \times \beta_C|$ as a function of Fermi energy for centre-bonded impurities. Solid (dashed) line corresponds to the case of unstrained (strained) impurities. Dashed line was obtained for a fixed value of strain, $\epsilon = 0.2$. Inset shows a log-scale plot of the difference between the two curves of the main panel plotted as a function of uniaxial strain for fixed values of Fermi energy. Solid line is for $E_F = 0$, dot-dashed line is for $E_F = 0.01t$ and dashed line is for $E_F = 0.05t$.

To illustrate this point, we evaluate the quantity $|\alpha_C \times \beta_C|$ under the action of uniaxial strain and plot it as a function of the Fermi energy, shown by the dashed line in the main panel of Fig. 6. For the sake of comparison, the solid line depicts the corresponding values for the strain-free case, as seen in Fig. 2. The inset shows the difference between the strained and unstrained cases plotted as a function of the uniaxial strain ϵ for three different values of Fermi energy. Note that a small amount of strain is sufficient to destroy the interference seen in the cross section of graphene doped with centre-bonded impurities. This is a different manifestation of the underlying physics to the orbital symmetry discussion presented in Ref. 27. Without the destructive interference in the scattering cross section the impurity transparency is lifted and centre-bonded dopants will act as strong scat-

terers just like the top-bonded counterparts. This is the ideal mechanism for sensitive strain sensors.

In summary, we have shown that the bonding symmetry of impurities in graphene can tell whether they act as strong or weak scatterers, regardless of their specificity. In particular, impurities that are top-bonded to the underlying hexagonal lattice are the most suitable for being chemically sensed by graphene. In contrast, centre-bonded impurities in graphene are invisible to conduction electrons and unable to scatter them. Nevertheless, any mechanism that breaks the perfect hexagonal symmetry of centre-bonded impurities will lift this invisibility, causing a subsequent enhancement of the resistivity in these materials. Mechanical strain is one obvious mechanism, which suggests that graphene doped with centre-bonded impurities are ideal candidates for high-sensitivity strain sensors. Finally, despite the simplicity of our model, it is worth emphasizing the generality of our finding. Having described the scattering of impurities through their self-energies, our conclusions are not dependent on specific choices of parameters but fundamentally dependent

on symmetry arguments. We argue that by classifying dopants according to their bonding symmetry leads to a more efficient way of identifying strong and weak scatterers. Rather than trial and error, our approach offers a major advance to establish which substances are good sensors for graphene. In the process of submitting our manuscript we learned of a work that obtains somewhat similar results by studying the conductivity corrections due to adsorbed impurities using the Kubo formula³⁷.

ACKNOWLEDGMENTS

C.L. thanks the financial support of the Brazilian funding agencies CNPq and FAPERJ. The Ireland-based authors acknowledge financial support from the Programme for Research in Third Level Institutions (PRTL). M.S.F. also acknowledges financial support from Science Foundation Ireland (Grant No. SFI 11/RFP.1/MTR/3083).

-
- ¹ A. K. Geim and K. S. Novoselov, “The rise of graphene,” *Nature Materials* **6**, 183–191 (2007).
 - ² A. K. Geim, “Graphene: Status and Prospects,” *Science* **324**, 1530–1534 (2009).
 - ³ A. H. Castro Neto, F. Guinea, N. M. R. Peres, K. S. Novoselov, and A. K. Geim, “The electronic properties of graphene,” *Rev. Mod. Phys.* **81**, 109 (2009).
 - ⁴ O. V. Yazyev, “Emergence of magnetism in graphene materials and nanostructures,” *Rep. Progr. Phys.* **73**, 056501 (2010).
 - ⁵ E. R. Mucciolo and C. H. Lewenkopf, “Disorder and electronic transport in graphene,” *J. Phys.: Condens. Matter* **22**, 273201 (2010).
 - ⁶ N. M. R. Peres, “*Colloquium* : The transport properties of graphene: An introduction,” *Rev. Mod. Phys.* **82**, 2673–2700 (2010).
 - ⁷ S. Das Sarma, S. Adam, E. H. Hwang, and E. Rossi, “Electronic transport in two-dimensional graphene,” *Rev. Mod. Phys.* **83**, 407 (2011).
 - ⁸ T. C. Li and S.-P. Lu, “Quantum conductance of graphene nanoribbons with edge defects,” *Phys. Rev. B* **77**, 085408 (2008).
 - ⁹ E. R. Mucciolo, A. H. Castro Neto, and C. H. Lewenkopf, “Conductance quantization and transport gaps in disordered graphene nanoribbons,” *Phys. Rev. B* **79**, 075407 (2009).
 - ¹⁰ J. P. Robinson, H. Schomerus, L. Oroszlány, and V. I. Fal’ko, “Adsorbate-limited conductivity of graphene,” *Phys. Rev. Lett.* **101**, 196803 (2008).
 - ¹¹ T. O. Wehling, M. I. Katsnelson, and A. I. Lichtenstein, “Adsorbates on graphene: Impurity states and electron scattering,” *Chem. Phys. Lett.* **476**, 125 (2009).
 - ¹² Shengjun Yuan, Hans De Raedt, and Mikhail I. Katsnelson, “Modeling electronic structure and transport properties of graphene with resonant scattering centers,” *Phys. Rev. B* **82**, 115448 (2010).
 - ¹³ D. Soriano, D. Van Tuan, S. M.-M. Dubois, M. Gmitra, A. W. Cummings, D. Kochan, F. Ortmann, J.-C. Charlier, J. Fabian, and S. Roche, “Spin transport in hydrogenated graphene,” *2D Materials* **2**, 022002 (2015).
 - ¹⁴ F. Schedin, A. K. Geim, S. V. Morozov, E. W. Hill, P. Blake, M. I. Katsnelson, and K. S. Novoselov, “Detection of individual gas molecules adsorbed on graphene,” *Nature Materials* **6**, 652–655 (2007).
 - ¹⁵ Rory Stine, Jeremy T. Robinson, Paul E. Sheehan, and Cy R. Tamanaha, “Real-Time DNA Detection Using Reduced Graphene Oxide Field Effect Transistors,” *Advanced Materials* **22**, 5297–5300 (2010).
 - ¹⁶ Ganhua Lu, Leonidas E. Ocola, and Junhong Chen, “Gas detection using low-temperature reduced graphene oxide sheets,” *Applied Physics Letters* **94**, 083111 (2009).
 - ¹⁷ J. T. Robinson, F. K. Perkins, E. S. Snow, Z. Wei, and P. E. Sheehan, “Reduced Graphene Oxide Molecular Sensors,” *Nano Letters* **8**, 3137–3140 (2008).
 - ¹⁸ Yuyan Shao, Jun Wang, Hong Wu, Jun Liu, Ilhan?A. Aksay, and Yuehe Lin, “Graphene based electrochemical sensors and biosensors: A review,” *Electroanalysis* **22**, 1027–1036 (2010).
 - ¹⁹ Q. He, S. Wu, Z. Yin, and H. Zhang, “Graphene-based electronic sensors,” *Chem. Sci.* **3**, 1764 (2012).
 - ²⁰ Shixin Wu, Qiyuan He, Chaoliang Tan, Yadong Wang, and Hua Zhang, “Graphene-based electrochemical sensors,” *Small* **9**, 1160–1172 (2013).
 - ²¹ Jingquan Liu, Zhen Liu, Colin J. Barrow, and Wenrong Yang, “Molecularly engineered graphene surfaces for sensing applications: A review,” *Anal. Chim. Acta* **859**, 1 (2015).
 - ²² O. Leenaerts, B. Partoens, and F. M. Peeters, “Adsorption of H₂O, NH₃, CO, NO₂, and NO on graphene: A first-principles study,” *Phys. Rev. B* **77**, 125416 (2008).
 - ²³ N. Gorjizadeh, A. A. Farajian, K. Esfarjani, and Y. Kawazoe, “Spin and band-gap engineering in doped graphene nanoribbons,” *Phys. Rev. B* **78**, 155427 (2008).

- ²⁴ T. O. Wehling, S. Yuan, A. I. Lichtenstein, A. K. Geim, and M. I. Katsnelson, “Resonant scattering by realistic impurities in graphene,” *Phys. Rev. Lett.* **105**, 056802 (2010).
- ²⁵ Jyoti Katoch, “Adatom-induced phenomena in graphene,” *Synthetic Metals* **210**, part A, 68 (2015).
- ²⁶ Héctor González-Herrero, José M. Gómez-Rodríguez, Pierre Mallet, Mohamed Moaied, Juan José Palacios, Carlos Salgado, Miguel M. Ugeda, Jean-Yves Veuillen, Félix Yndurain, and Iván Brihuega, “Atomic-scale control of graphene magnetism by using hydrogen atoms,” *Science* **352**, 437 (2016).
- ²⁷ B. Uchoa, T. G. Rappoport, and A. H. Castro Neto, “Kondo quantum criticality of magnetic adatoms in graphene,” *Phys. Rev. Lett.* **106**, 016801 (2011).
- ²⁸ J. H. García, B. Uchoa, L. Covaci, and T. G. Rappoport, “Adatoms and Anderson localization in graphene,” *Phys. Rev. B* **90**, 085425 (2013).
- ²⁹ E. N. Economou, *Green’s Functions in Quantum Physics*, 3rd ed. (Springer, Berlin, 2006).
- ³⁰ S. R. Power and M. S. Ferreira, “Electronic structure of graphene beyond the linear dispersion regime,” *Phys. Rev. B* **83**, 155432 (2011).
- ³¹ C. Bena and G. Montambaux, “Remarks on the tight-binding model of graphene,” *New J. Phys.* **11**, 095003 (2009).
- ³² P. A. Lee and D. S. Fisher, “Anderson Localization in Two Dimensions,” *Phys. Rev. Lett.* **47**, 882 (1981).
- ³³ J. Mathon, A. Umerski, and M. Villeret, “Oscillations with Co and Cu thickness of the current-perpendicular-to-plane giant magnetoresistance of a Co/Cu/Co(001) trilayer,” *Phys. Rev. B* **55**, 14378 (1997).
- ³⁴ A. T. Costa, M. S. Ferreira, Toby Hallam, Georg S. Duesberg, and A. H. Castro Neto, “Origami-based spintronics in graphene,” *EPL (Europhysics Letters)* **104**, 47001 (2013).
- ³⁵ C. H. Lewenkopf and E. R. Mucciolo, “The recursive Green’s function method for graphene,” *J. Comput. Electron.* **12**, 203 (2013).
- ³⁶ V. M. Pereira, A. H. Castro Neto, and N. M. R. Peres, “Tight-binding approach to uniaxial strain in graphene,” *Phys. Rev. B* **80**, 045401 (2009).
- ³⁷ D. A. Ruiz-Tijerina and L. G. G. V. Dias da Silva, “Symmetry-protected coherent transport for diluted vacancies and adatoms in graphene,” ArXiv e-prints (2016), arXiv:1606.00742 [cond-mat.mes-hall].